[superscript 19]F-labeling of the adenine H2-site to study large RNAs by NMR spectroscopy

Citation: Sochor, F., R. Silvers, D. Müller, C. Richter, B. Fürtig, and H. Schwalbe. "19F-Labeling of the Adenine H2-Site to Study Large RNAs by NMR Spectroscopy." J Biomol NMR 64, no. 1 (December 24, 2015): 63–74.

As Published: http://dx.doi.org/10.1007/s10858-015-0006-9

Publisher: Springer Netherlands

Persistent URL: http://hdl.handle.net/1721.1/105512

Version: Author's final manuscript: final author's manuscript post peer review, without publisher's formatting or copy editing

J Biomol NMR (2016) 64:63–74
DOI 10.1007/s10858-015-0006-9

ARTICLE

^{19}F-labeling of the adenine H2-site to study large RNAs by NMR spectroscopy

F. Sochor[1] · R. Silvers[1,2] · D. Müller[1] · C. Richter[1] · B. Fürtig[1] · H. Schwalbe[1]

Received: 13 October 2015 / Accepted: 20 December 2015 / Published online: 24 December 2015

Abstract In comparison to proteins and protein complexes, the size of RNA amenable to NMR studies is limited despite the development of new isotopic labeling strategies including deuteration and ligation of differentially labeled RNAs. Due to the restricted chemical shift dispersion in only four different nucleotides spectral resolution remains limited in larger RNAs. Labeling RNAs with the NMR-active nucleus ^{19}F has previously been introduced for small RNAs up to 40 nucleotides (nt). In the presented work, we study the natural occurring RNA aptamer domain of the guanine-sensing riboswitch comprising 73 nucleotides from *Bacillus subtilis*. The work includes protocols for improved in vitro transcription of 2-fluoroadenosine-5′-triphosphat (2F-ATP) using the mutant P266L of the T7 RNA polymerase. Our NMR analysis shows that the secondary and tertiary structure of the riboswitch is fully maintained and that the specific binding of the cognate ligand hypoxanthine is not impaired by the introduction of the ^{19}F isotope. The thermal stability of the ^{19}F-labeled riboswitch is not altered compared to the unmodified sequence, but local base pair stabilities, as measured by hydrogen exchange experiments, are modulated. The characteristic change in the chemical shift of the imino resonances detected in a ^{1}H,^{15}N-HSQC allow the identification of Watson–Crick base paired uridine signals and the ^{19}F resonances can be used as reporters for tertiary and secondary structure transitions, confirming the potential of ^{19}F-labeling even for sizeable RNAs in the range of 70 nucleotides.

Keywords ^{19}F-NMR · Riboswitch · In vitro transcription · 2F-ATP

Introduction

Nuclear magnetic resonance (NMR) spectroscopy has a considerable impact for the determination of structure of functional RNA molecules. Further, it is unique in describing RNA dynamics at atomic resolution (Butcher et al. 2000; Carlomagno et al. 2013; Chowdhury et al. 2006; D'Souza et al. 2004; Davis et al. 2005; Duszczyk et al. 2011; Ferner et al. 2009; Furtig et al. 2003; Houck-Loomis et al. 2011; Keane et al. 2015; Marchanka et al. 2015; Sashital et al. 2004; Staple and Butcher 2003; Wacker et al. 2011). In fact, dynamics ranging from sub nanoseconds to seconds have been found to be essential to understand RNA function (Buck et al. 2007; Rinnenthal et al. 2011).

One considerable obstacle to NMR spectroscopic studies is its size limitation due to linewidth and limited chemical shift resolution. Spectra of RNA have limited chemical shift dispersion. With the exception of imino signals the NMR resonance of the only four different RNA nucleotides resonate in a narrow spectral regime. The

Electronic supplementary material The online version of this article (doi:10.1007/s10858-015-0006-9) contains supplementary material, which is available to authorized users.

✉ B. Fürtig
fuertig@nmr.uni-frankfurt.de

✉ H. Schwalbe
schwalbe@nmr.uni-frankfurt.de

[1] Institut für Organische Chemie und Chemische Biologie, Center for Biomolecular Magnetic Resonance (BMRZ), Johann Wolfgang Goethe-University Frankfurt, Max-von-Laue-Str. 7, 60438 Frankfurt/M., Germany

[2] Present Address: Department of Chemistry, Francis Bitter Magnet Laboratory, Massachusetts Institute of Technology, Cambridge, MA 02139, USA

limited chemical shift dispersion has—in part—been overcome by multidimensional heteronuclear NMR in combination with uniformly labeling approaches using ^{13}C, ^{15}N and ^{2}H labeled nucleotides in T7 RNA polymerase mediated in vitro transcription (Alvarado et al. 2014; Batey et al. 1992; Dayie et al. 1998; Furtig et al. 2008; Nikonowicz et al. 1992; Thakur and Dayie 2012) and position specific labeling using chemical synthesis (Kline and Serianni 1990; Neuner et al. 2015; Quant et al. 1994; Wenter et al. 2006).

One possibility to overcome limited spectral resolution is to introduce additional nuclei that have similar NMR properties compared to ^{1}H. The ^{19}F isotope has been used in protein and RNA studies, as it has 100 % natural abundance, its gyromagnetic ratio is 0.94 that of ^{1}H, reveals a chemical shift dispersion comparable to that of ^{1}H, and ^{19}F-NMR spectroscopy has become a very useful tool for the analysis of large structures and dynamic systems, e.g. peptide nucleic acid building blocks but also in ligand screening by NMR spectroscopy (Garavis et al. 2014; Kiviniemi et al. 2013).

The use of fluorinated nucleotides has already been introduced in 1964: Codington et al. first synthesized 2′F-subtituted nucleotides (Codington et al. 1964) and, subsequently, uniformly 2′F-labeled RNAs were synthesized (Suck et al. 1974). The advantages of ^{19}F-labeled RNAs for NMR spectroscopic applications were first described in the early 1970s (Horowitz et al. 1974). *E. coli* cultures were grown in medium containing 5-fluorouracil. This approach yielded RNAs with a 5-fluorouracil substitution up to 93 %. The labeling did not affect the RNA structure or function and allowed the determination of the valine-tRNA recognition sites of the cognate aminoacyl-tRNA synthetase by ^{19}F-NMR spectroscopy. Since then, 2′F-labeled nucleotides have become widely used in solid-state and liquid-state NMR spectroscopy (Kreutz et al. 2005; Olsen et al. 2005). The modification on the ribosyl moiety of nucleotides allows the use of one similar labeling schema for all nucleobases. Using the 2′-deoxy-2′-trifluoromethylthio (SCF3) unit or other highly fluorinated substitutions can even enhance the sensitivity of ^{19}F-NMR spectroscopy (Fauster et al. 2012; Kiviniemi and Virta 2010; Kosutic et al. 2014), in particular for large RNAs. However, uniform labeling of the RNA with 2′F-substituted nucleotides can disrupt tertiary interactions that involve the 2′OH group and shift the conformational preferences of the ribofuranosyl sugar unit to preferentially adopt the 3′-endo conformation and therefore influences the structural behavior (Reif et al. 1997). The use of other labeling positions than 2′ can overcome the 3′-endo preference in uniformly labeled RNAs without losing the advantage of ^{19}F-NMR spectroscopy (Granqvist and Virta 2014; Puffer et al. 2009). ^{19}F-labeled nucleotides are often introduced by chemical synthesis which provides a single introduction of the label at a defined position within the RNA of interest. ^{19}F-nuclei are very sensitive to environmental changes such as differences in the secondary structure or ligand binding (Kreutz et al. 2005, 2006). Together with the rather small size of the label it represents a very useful tool for the analysis of bistable RNAs, weak complexes, or large ligand binding RNAs (Graber et al. 2008; Kiviniemi and Virta 2011).

Compared to chemical synthesis, in vitro transcription allows synthesis of much larger RNAs. In order to couple the advantages of the enzymatic based in vitro transcription with those of ^{19}F-NMR, fluorinated reporter molecules or ligands can be used while the RNA stays unmodified (Lombes et al. 2012). However, direct measurements of structural and dynamic changes require an appropriated label within the RNA. In 2004, Scott et al. showed that 2F-ATP (Fig. 1b), which was produced using a combination of *E. coli* cultured in growth medium supplemented with 9-β-D-arabinofuranosyl-2-fluoroadenine and further enzymatic modification (Baldo et al. 1983; Huang and Plunkett 1987), could be incorporated into HIV-2 TAR (9 kDa) by in vitro transcription (Scott et al. 2004). ^{19}F-NMR spectroscopy allowed the identification of the substituted nucleotides and showed that the label did not affect the structural integrity or thermodynamic stability of the RNA. Their work coupled the advantages of in vitro transcription with full fluorination of the RNA molecule which allows the direct measurement of structural changes during ligand binding. However, substitution of the H2 by ^{19}F changes the polarization of the nucleobase and can potentially disrupt RNA motifs that are based on van-der-Waals interactions such as the A-minor motif (Lescoute and Westhof 2006; Nissen et al. 2001). This minor-groove triplex is based on tertiary base–base and base-backbone interactions including the adenine nucleobase atoms N1, C2, N3 and the ribose 2′-OH group. For such RNA structural motif, the effect of the introduction of the ^{19}F-label needs to be carefully investigated.

Here, we apply ^{19}F-labeling to study RNA riboswitches. RNA riboswitches are structured gene regulation elements located in the 5′-untranslated region (5′-UTR) of mRNAs (Nahvi et al. 2002). The term riboswitch refers to its function to activate or repress gene expression by a conformational transition of the riboswitch RNA mediated through the interaction commonly with a low-molecular-weight ligand. Central to ligand binding is the aptamer domain that, upon addition of ligand (Schwalbe et al. 2007), is stabilized in a secondary and tertiary structure that leads to an allosteric conformational switch of secondary structure elements that activate or interfere with either transcription or translation. The binding to either guanine or hypoxanthine to the *xpt–pbuX* riboswitch (Gsw)

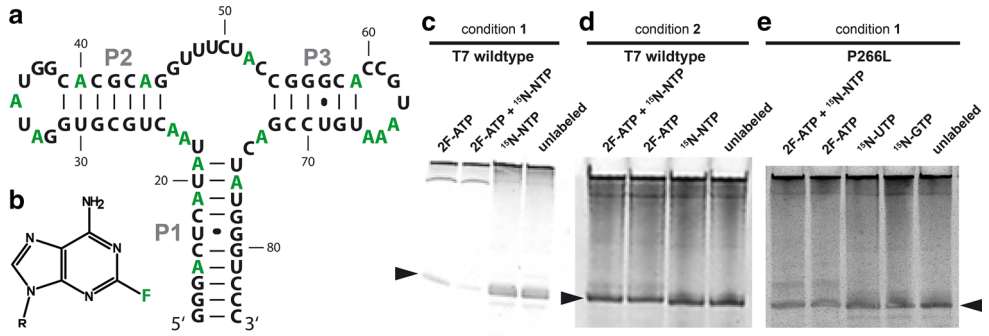

Fig. 1 **a** Secondary structure of the Gsw^{apt}. The ^{19}F-labeled adenines are indicated in green. **b** Structure of the fluorinated base of 2F-ATP. The ribosetriphosphate is indicated by the R. **c** 10 % PAGE of transcriptions using condition **1** with wildtype T7 RNA polymerase. The 73mer is indicated by the black arrow. The title indicates if 2F-ATP substituted ATP or ^{15}N-labeled NTPs were used for transcription. **d** 10 % PAGE of transcriptions using condition **2** with wildtype T7 RNA polymerase. **e** 10 % PAGE of transcriptions using condition **1** with P266L T7 RNA polymerase

from *Bacillus subtilis* for example adopts two exclusive secondary structures acting as terminator and anti-terminator signals of DNA-templated RNA transcription (Mandal et al. 2003).

We uniformly labeled the aptamer domain (Noeske et al. 2005) of the guanine sensing riboswich (Gsw^{apt}, 22 kDa, Fig. 1a) with 2F-ATP by a T7 RNA polymerase based in vitro transcription and showed that neither the structural integrity nor the ligand binding ability of the aptamer were affected by the F2 label as stabilizing and destabilizing effects compensate each other. As riboswitches work through a ligand concentration depending switching mode, labeling adenosine nucleotides at the C2 position with ^{19}F is a promising approach for the investigation of the switching process in real time by ^{19}F-NMR spectroscopy.

Materials and methods

Synthesis

Milligram quantities of 2F-adenine labeled and unlabeled Gsw^{apt} (73-nt) were synthesized by in vitro transcription from linearized plasmid DNA (**TAA TAC GAC TCA CTA TA***G GGA CTC ATA TAA CTG CGT GGA TAT GGC ACG CAG GTT TCT ACC GGG CAC CGT AAA TGT CCG ACT ATG GGT CCC*) using the P266L mutant of T7 RNA polymerase (Guillerez et al. 2005). The in vitro transcription (total volume 18 mL) was performed in 100 mM Tris-glutamate buffer pH 8.2, 25 mM $Mg(OAc)_2$, 25 mM NTPs (22 % A, 26 % C, 29 % G, 23 % U; for ^{15}N-labeling, ^{15}N-GTP and ^{15}N-UTP were used), 20 mM DTT, 2 mM spermidine, 50 ng/µL DNA (linearized using *SmaI*), and 70 µg/mL P266L. 2F-ATP was purchased at the Jena Bioscience GmbH (Jena, Germany). After transcription, the RNA was pre-purified by a DEAE Sepharose column equilibrated with 0.1 M NaOAc. The NaOAc concentrations used for washing were 0.1, 0.6 and 1 M. The RNA was eluted with 2 M and 3 M NaOAc, ethanol precipitated, and further purified by reversed phase HPLC using a Perfectsil RP18 10 × 250 mm column. A 50 mM potassium phosphate buffer pH 5.9 (Buffer A) was used for equilibration. For elution, Buffer A + 60 % acetonitrile (Buffer B) was used in a gradient. The RNA was eluted between 40 and 50 % Buffer B. After precipitation, the RNA was washed with and solved in water, refolded by heating to 95 °C for 5 min and rapid cooling on ice. The concentration was determined by UV (ε_{260} = 792.55 L mmol^{-1} cm^{-1} (Cavaluzzi and Borer 2004)) and homogeneity was analyzed by native polyacrylamide gel electrophoresis (PAGE).

For the CD- and NMR-measurements, the RNA was dissolved in a buffer containing 25 mM potassium phosphate pH 6.5 and 50 mM KCl to OD_{260} = 0.3. NMR samples contained 90:10 H_2O:D_2O. For CD-measurements, the ligand hypoxanthine (Christiansen et al. 1997; Mandal et al. 2003) was added in 20-fold excess to the labeled and unlabeled Gsw^{apt}. Due to the low hypoxanthine solubility, the ligand was added together with 2 mM Mg^{2+} in a ten-fold excess to the labeled Gsw^{apt} for the ^{1}H,^{1}H-NOESY and ^{19}F,^{1}H-HOESY experiments (0.2–0.3 mM RNA).

Circular dichroism spectroscopy (CD)

All spectra were recorded on a CD- spectrometer J-810 (JASCO) in a thermostatic cuvette holder. Samples were placed in quartz cuvettes with a pathway length of 1 cm and a sample volume of 800 µL. Baseline correction was applied by subtracting a spectrum recorded on plain buffer solution. The acquisition parameters were set to a wavelength range of 300–190 nm and a bandwidth of 1 nm. Displayed spectra were recorded with 3 scans each. The temperature was raised from 5 to 95 °C in 0.5 °C steps.

Each temperature was kept constant for 20 s before the measurement was started. The absorption maximum of the RNA samples was observed at 264 nm.

NMR spectroscopy

All 1D proton spectra were measured at 295 K using Bruker 600, 800, 900 and 950 MHz spectrometer equipped with a cryogenic z-gradient HCN probe. Water suppression was achieved by application of jump-return pulse trains (Sklenar and Bax 1987). Proton pulses were applied on-resonance at the water frequency with field strength between 19 kHz and 22 kHz. For static measurements, 512 transients were averaged, the relaxation delay was set to 1 s, and the spectral width was 25 ppm. Gradients had a smoothed square shape and were applied with strength of 90 %. Decoupling was achieved using GARP-sequence (Shaka et al. 1985).

For the assignment of imino proton resonances, jump-return-NOESY (Sklenar and Bax 1987) spectra were recorded at 295 K. All jump-return-NOESY spectra were recorded using Bruker 900 and 950 MHz spectrometers equipped with a cryogenic z-gradient HCN probe. Hard pulses were applied, using a frequency jump, with t_1 at the midpoint of all RNA proton resonances (7.5 ppm) and t_2 on water resonance prior to the mixing period for detection with field strength of 18 kHz. Spectra were recorded with a spectral width of 15 ppm and 25 ppm for the indirect and direct dimensions; 512 and 2048 pts were recorded for t_1 and t_2, respectively. Gradients had a sinusoidal shape and were applied with strength of 90 %. Decoupling was achieved using GARP-sequence. The relaxation delay was set to 1.5 s and the mixing time was set to 150 ms.

The ^{1}H,^{15}N-HSQCs [FHSQC (Mori et al. 1995)] utilizing binominal Watergate (Piotto et al. 1992; Sklenar et al. 1993) scheme for water suppression were recorded at 295 K using a Bruker 600 MHz equipped with a cryogenic z-gradient HCN probe. Proton pulses were applied on-resonance at the water frequency with field strength of 22 kHz. Spectra were recorded with a spectral width of 22 and 25 ppm for the indirect and direct dimensions; 256 and 2048 pts were recorded for t_1 and t_2, respectively. Proton pulses were applied on-resonance at the water frequency with field strength of 22.5 kHz. ^{15}N decoupling during acquisition was achieved using GARP-sequence.

The imino proton exchange rates were measured at 298 K and fitted using sigma plot as previously described (Rinnenthal et al. 2010) at a Bruker 600 MHz with a pseudo 3D ^{1}H,^{15}N-HSQC using exchange times of 80 µs, 1 ms, 50, 100, 250, 500, 750, 1000, 2000, 4000 ms. Selective inversion of the water resonance was achieved by application of 2 ms shaped pulses with RE-BURP (Geen and Freeman 1991) profile. ^{15}N decoupling during acquisition was achieved using GARP-sequence.

The recorded parameters were fitted using the quotient of the intensity of the imino proton signal at the time t_m (mixing time) and the intensity of the imino proton signal at the time $t_m = 0$ in the y-axis and t_m in the X-axis.

All 1D ^{19}F spectra were measured at 295 K using Bruker 300 and 500 MHz spectrometer. The 300 MHz was equipped with a BBFO probe where the ^{1}H and the ^{19}F nuclei are measured at separated coils whereas the 500 MHz was equipped with a BBO prodigy probe where the ^{1}H and the ^{19}F nuclei are measured at the same coil. ^{19}F pulses were applied at −52 ppm with field strength between 23.1 and 16.7 kHz. For static measurements, 256 transients were averaged, the relaxation delay was set to 1 s, and the spectral width was 100 ppm.

The ^{19}F,^{1}H-Heteronuclear NOESY [HOESY,(Yu and Levy 1984)] spectra were recorded using the Bruker 300 MHz. ^{19}F pulses were applied at −52 ppm with field strength of 23.1 kHz. The proton pulse was applied on-resonance at the water frequency with field strength of 22.2 kHz. Spectra were recorded with a spectral width of 10.5 and 20 ppm for the indirect and direct dimensions; 128 and 2048 pts were recorded for t_1 and t_2, respectively. Decoupling was achieved using MLEV-sequence (Levitt and Freeman 1981). The relaxation delay was set to 2 s and the mixing time was set to 200 ms.

Results

Optimizing synthesis

We first synthesized the Gsw^{apt} (Fig. 1c) by in vitro transcription using the wild type T7 RNA polymerase under condition **1** (100 mM Tris-Glutamate pH 8.2, 20 mM DTT, 2 mM spermidine, 70 µg/mL T7 RNA polymerase: concentrations of $Mg(OAc)_2$, DNA template and NTPs were optimized). Upon addition of 2F-ATP, a decrease in incorporation efficiency was observed. Changing to condition **2** used by Scott et al. (Milligan et al. 1987; Scott et al. 2004) (40 mM Tris–HCl pH 8.1, 5 mM DTT, 1 mM spermidine, 50 µg/mL BSA, 0.1 % triton X-100, 80 mg/mL PEG, 0.002 U/µL pyrophosphatase; 70 µg/mL T7 RNA polymerase: concentrations of $Mg(OAc)_2$, DNA template and NTPs were optimized) resulted in an comparable incorporation efficiency for unlabeled nucleotides and 2F-ATP (Fig. 1d). The incorporation efficiency was 6.0 % for unlabeled nucleotides under condition **2** whereas the incorporation efficiency was 4.7 % for 2F-ATP under the same conditions. This resulted in an insufficient yield for NMR samples. We therefore changed to the P266L mutant of the T7 RNA polymerase. Under condition **1**, the incorporation efficiency of 2F-ATP was 21.1 % compared to 31.1 % of the unlabeled NTPs (Fig. 1e). This incorporation

efficiency allowed us to synthesize the RNA in sufficient amounts for our NMR measurements. The use of condition **2** for P266L did not result in higher incorporation efficiencies. Our data suggest that compared to the wildtype T7 RNA polymerase and under condition **1**, the P266L mutant has superior incorporation abilities of 2F-ATP. Whether the mutant possesses further advantages regarding the incorporation of modified nucleotides remains to be investigated.

In vitro transcription under condition **1** (total volume: 18 mL with 0.986 mL 100 mM 2F-ATP) using P266L resulted in a single 73mer. No transcription abortion products were identified in the used 10 % PAGE stained with GelRed, that has a detection limit of 0.1 ng nucleic acid. Purification and refolding yielded in total 0.1 µmol of RNA. The NMR sample had a concentration of 0.3 mM and a very high homogeneity.

Global stability

In order to investigate the effect of the 2F-ATP substitution on the structural stability and on ligand binding, CD-melting curves of the ^{19}F-labeled and unlabeled aptamers, in the presence and absence of ligand were recorded (Fig. 2). The shape of the temperature dependent CD-curves of the unlabeled and ^{19}F-labeled RNAs were found to be very similar in the absence and presence of ligand (Fig. 2a). The first order derivatives (Fig. 2b) showed that in the absence of ligand, the RNAs have distinct melting points [T_m(RNA) 65.7 ± 0.4 °C; T_m(^{19}F-RNA) 67.2 ± 0.4 °C]. When ligand is added, both RNAs show an identical change of shape of their first order derivatives. The melting points are shifted to T_m(RNA) 69.9 ± 0.6 °C and T_m(^{19}F-RNA) 68.8 ± 0.5 °C. The stabilization effect of ligand binding was similar for both aptamers.

As both RNAs show identical results within error and undergo the same thermodynamic changes, it can be concluded that the incorporation of 2F-ATP does not affect the structural integrity of the RNA significantly, in accordance with previous studies on different RNA systems (Scott et al. 2004). We further demonstrated that the ligand binding of the aptamer is not impaired by the ^{19}F-label.

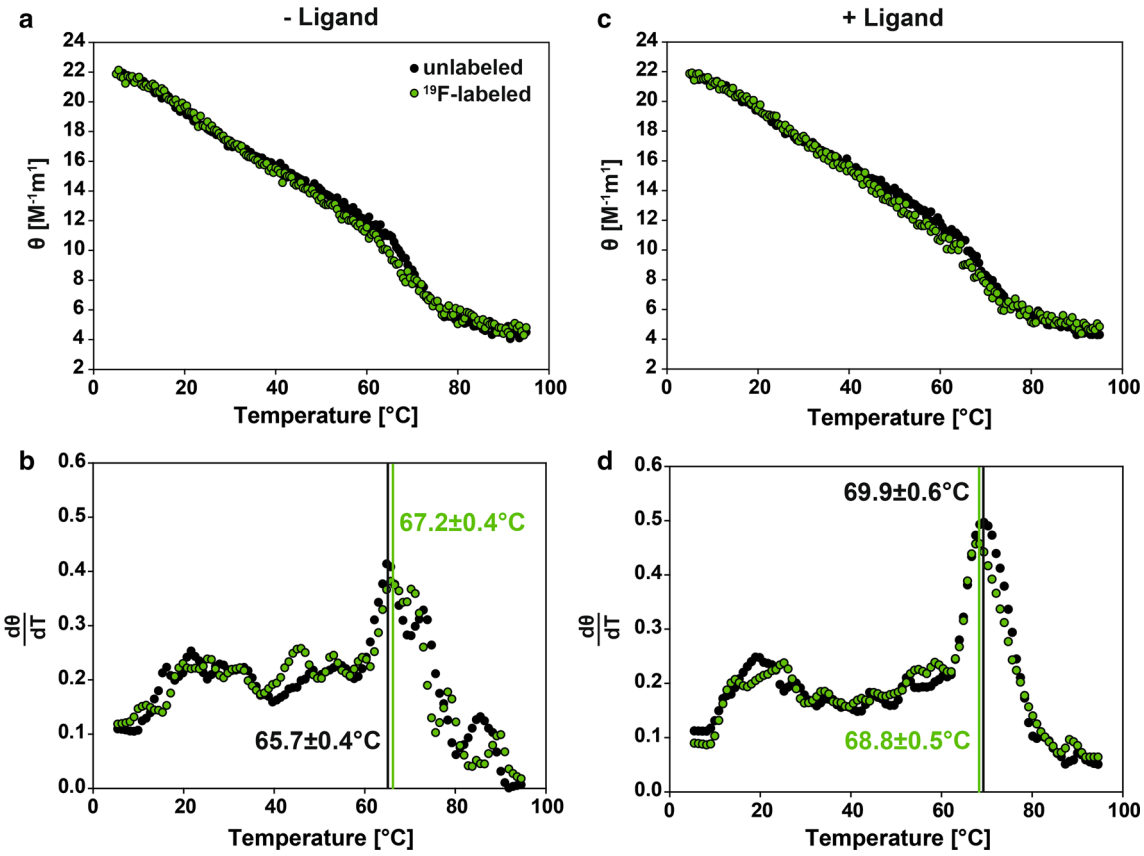

Fig. 2 **a**, **b** CD-melting curves and first order derivatives of the ^{19}F-labeled (*green*) and unlabeled (*black*) Gsw^{apt} in the absence of ligand. The melting points are indicated. For the CD-melting curve, the molar ellipticity (Θ) was plotted against the temperature (T). For the first order derivative, the derivation of Θ against T was plotted against the temperature. **c**, **d** CD-melting curves and first order derivatives of the ^{19}F-labeled (*green*) and unlabeled (*black*) Gsw^{apt} in the presence of ligand. The melting points are indicated. For the CD-melting curve, the molar ellipticity (Θ) was plotted against the temperature (T). For the first order derivative, the derivation of Θ against T was plotted against the temperature

Assignment

The assignment of the imino protons of the ^{19}F-labeled RNA and the unlabeled reference were obtained from ^{1}H,^{1}H-NOESY (Supplementary Fig. 8) and ^{1}H,^{15}N-HSQC experiments. The overlaid ^{1}H,^{15}N-HSQCs are shown in Fig. 3a. The signals of the guanine and uridine imino protons involved in G-U base pairing are shifted in the proton dimension by an average of 0.1 ppm which is within the range of the peak width of 0.15 ppm (Fig. 3b). The shift change of these protons is therefore considered to be negligible. The only signal of the imino protons involved in G–C pairing that undergoes a significant shift is G56 ($\Delta\delta^{1}H = 0.45$ ppm). This could be due to the lower stability of the helix P3 compared to the helix P1. The signals of the ^{19}F-labeled aptamer show an average high-field shift of $<\Delta\delta^{1}H> = -2.5$ ppm in the uridine imino proton region for all uridine protons which are involved in base pairing to 2F-adenine. This lies within the reported range of $<\Delta\delta^{1}H> = -2.6$ ppm (Scott et al. 2004).

Local stability

In order to investigate the influence of the ^{19}F-label on individual base pair stability, we measured the exchange rates of the imino protons with water located in the P1 (10 base pairs) and P3 (6 base pairs) helices (Supplementary Table 1). One G–U wobble base pair is situated in the middle of each of the helices whereas the base is composed of three G–C base pairs. Upon introduction of the ^{19}F-label for base pairs of the same pairing scheme consistent changes in the exchange curves of the imino protons are observed. More pronounced changes are detectable for the exchange behavior of imino proton stemming from helix P1 compared to those from helix P3.

For all analyzed imino protons, the minimum of the curve is less negative when ^{19}F is introduced into the RNA (Fig. 4). The minima of the exchange curves of all imino protons are shifted to smaller τ_m upon labeling of the RNA. Only the exchange curve of the adenine paired U81 is shifted to higher τ_m. The changes of signal intensity in the helix P1 are more pronounced than in helix P3. This could be caused by the number of base pairs or the number of modified adenines which are involved in the helix formation.

The exchange rates of the imino protons in the helices P1 and P3 are shown in Fig. 5a. In the helix P1, the exchange rate of the imino proton of G14 and G80 which are involved in G–C base pairing are slightly decreased by $\Delta k_{ex} = -0.16\ s^{-1}$ and $\Delta k_{ex} = -0.56\ s^{-1}$, respectively, when the ^{19}F-label is introduced. This indicates that in the ^{19}F-labeled RNA the exchange is slower than in the unlabeled form. The exchange rates of U81 which is situated between G14 and G80 is the only uridine imino proton whose exchange rate is significantly decreased ($\Delta k_{ex} = -4.02\ s^{-1}$) compared to the unlabeled RNA. This

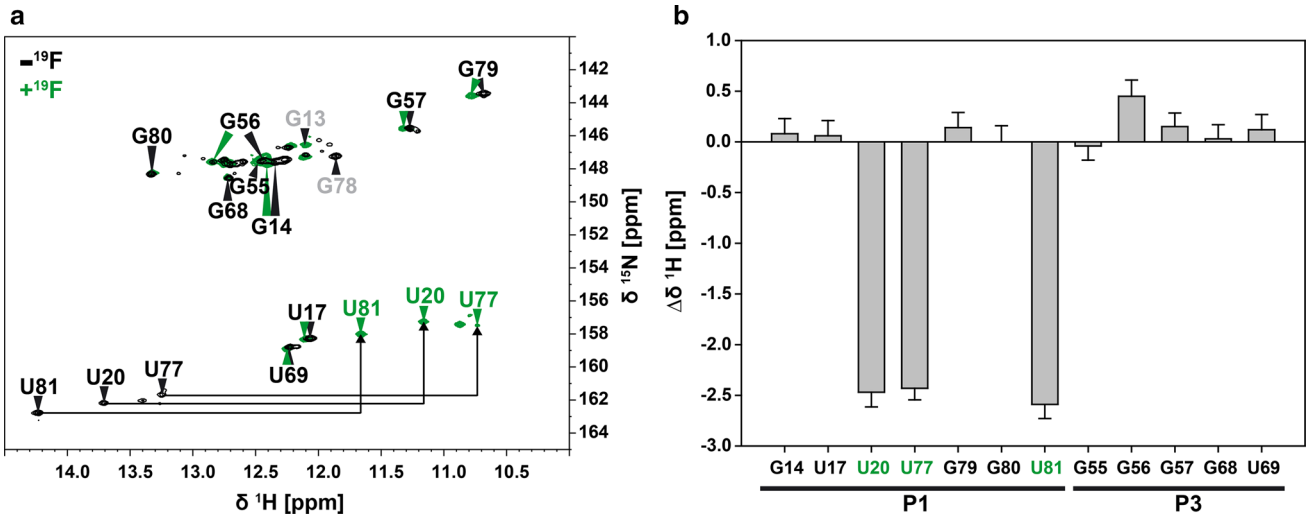

Fig. 3 a Spectrum of the G and U imino proton region of a proton detected ^{1}H,^{15}N-HSQC of the ^{15}N-labeled (*black*) and ^{19}F-^{15}N-double labeled (*green*) Gsw^{apt} at the 600 MHz and 298 K. The ^{1}H pulses were applied at the water frequency. The carrier for ^{15}N was set to 151 ppm. For hard ^{1}H and ^{15}N pulses, field strengths of 22 kHz and 7.1 kHz were used, respectively. During acquisition, ^{15}N decoupling was achieved by GARP-decoupling. The 2D experiment was recorded with a spectral width of 22 and 25 ppm for the indirect and direct dimension, respectively; 256 and 2048 pts were recorded for t_1 and t_2, respectively. The relaxation delay was set to 1 s. The signals assigned in both spectra are indicated in black, the signals assigned in both spectra but shifted in the spectrum of the ^{19}F-labeled RNA are shown in green and the signals assigned in only one of the spectra are shown in grey. **b** Signal shift of the imino proton signals in the ^{1}H dimension between the unfluorinated and the fluorinated RNA. The error bars are derived from the lane width of the signals. The adenine paired uridines are labeled in green. The helices P1 and P3 are indicated

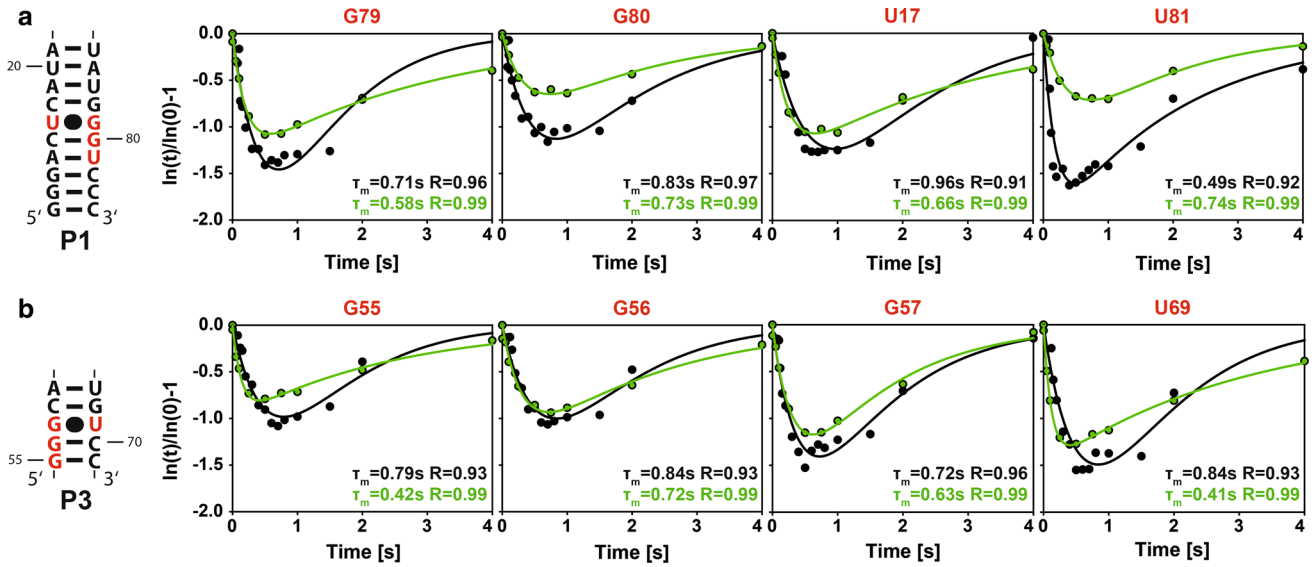

Fig. 4 **a** Imino proton exchange of hydrogen bonds situated in the helix P1 in the unlabeled (*black*) and ^{19}F-labeled (*green*) Gsw^{apt}. The nucleobase corresponding to the exchanged imino proton is indicated on top of each blot (*red*). The helices (P1 and P3) containing the nucleobase whose imino protons' exchange behavior is shown are represented on the left hand side (*red*). The R-value and τ_m are indicated for the imino protons of the unlabeled (*black*) and labeled (*green*) RNA. **b** Imino proton exchange hydrogen bonds situated in the helix P3 in the unlabeled (*black*) and ^{19}F-labeled (*green*) Gsw^{apt}

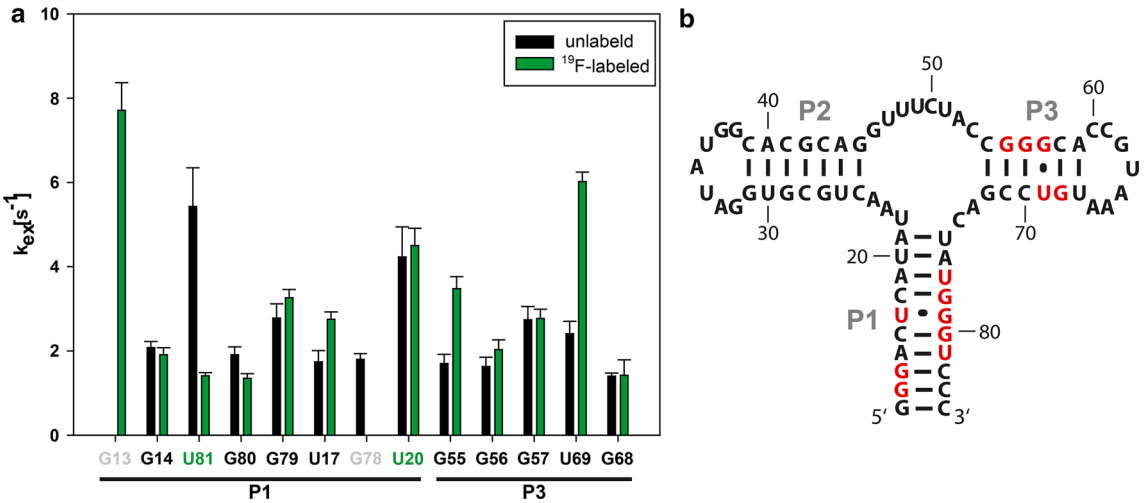

Fig. 5 **a** Exchange rates of the imino protons involved in the base pair formation of the helices P1 and P3. **b** Schematic representation of the secondary structure of Gsw^{apt} with the indicated nucleotides whose exchange rates were measured (*red*)

could be caused by the stabilizing G–C base pairs G14 and G80. The exchange rates of U20, which is involved in A–U base pairing, increases when paired to a 2F-adenine (U20: $\Delta k_{ex} = 0.27\ s^{-1}$). The exchange rates of the imino protons of uridines paired to adenines are highly increased when the uridines are paired to a 2F-adenine. The exchange rates of G79 and U17 are increased of $\Delta k_{ex} = 0.48$ and $\Delta k_{ex} = 1.01\ s^{-1}$, respectively, when the label is introduced. Nevertheless, all imino protons which are not involved in G–C base pairing seem to be destabilized by the ^{19}F-label, even when not directly paired to 2F-adenine.

Contrarily to the helix P1, the exchange rates of the imino protons in the helix P3 which are involved in G–C base pairing (G55: $\Delta k_{ex} = 1.78\ s^{-1}$ and G56: $\Delta k_{ex} = 0.40\ s^{-1}$, G68 $\Delta k_{ex} = 0.02\ s^{-1}$) show an increase. The G-U wobble base pair, G57 and U69, shows an increase of the exchange rate of $\Delta k_{ex} = 0.03$ and $\Delta k_{ex} = 3.61\ s^{-1}$, respectively, which is comparable to the

G–U base pair in the helix P1. The uridine imino protons of the wobble base pairs seem to be more destabilized upon addition of the ^{19}F-label than the guanine imino protons.

The exchange behavior of the imino protons is influenced by the accessibility of the solvent and the NOE to nearby nuclei. The introduction of ^{19}F in a close position to the hydrogen bonds can influence the calculated exchange rates by NOE even if the gyromagnetic ratios of ^{1}H and ^{19}F are close. As a result, the exchange rates of the imino protons in the ^{19}F-labeled RNA can appear larger. However, as was shown before, the ^{19}F-labeling of the aromatic system in RNA nucleobases can have two opposing effects. The base pairing stability is decreased (Broom et al. 1979) whereas the base stacking is increased (Battaglia et al. 1981). These two opposing effects can compensate each other so that the overall stability of the RNA is not impaired.

Ligand binding to ^{19}F-labeled Gsw^{apt}

Ligand binding to the ^{19}F-labeled Gsw^{apt} was analyzed by ^{1}H,^{1}H-NOESYs. The spectrum without ligand is shown in Fig. 6a. G80, U81, U20 and U77 were used as reference peaks and, compared to the unlabeled RNA, the A-U base paired imino protons show a $<\Delta\delta^{1}H> = -2.6$ ppm in the ^{19}F-labeled RNA. Ligand binding to the RNA is shown by the H1 signal of hypoxanthine (Fig. 6b), which is protected from exchange when bound, and by the reporter signals from the binding pocket U22 and U47 (Wacker et al. 2012). In the ligand unbound state, U22 is Watson–Crick paired to A52 (Serganov et al. 2004). Upon ligand binding, this base pair remains intact and U22 additionally coordinates to the ligand by the 2′-OH group of the ribose. Due to the unaffected A–U base pairing, the imino proton signal of U22 is shifted ($\Delta\delta^{1}H = -2.4$ ppm) in the ^{19}F-labeled RNA. U47 is situated in the binding pocket but does not form a canonical base pair. Upon ligand binding, U47 coordinates to the ligand. In the ^{19}F-labeled RNA, its imino proton signal does not show a shift in the proton dimension. In the absence of Mg^{2+}, the Gsw^{apt} conformation is characterized by pre-formed loop–loop interactions (Buck et al. 2010). Addition of Mg^{2+} stabilizes these tertiary interactions. Upon ligand and Mg^{2+} binding, the imino proton of U34 (Wacker et al. 2012), which forms a reverse Hoogsteen base pair to A65 (Serganov et al. 2004), becomes protected from exchange and is therefore visible in the

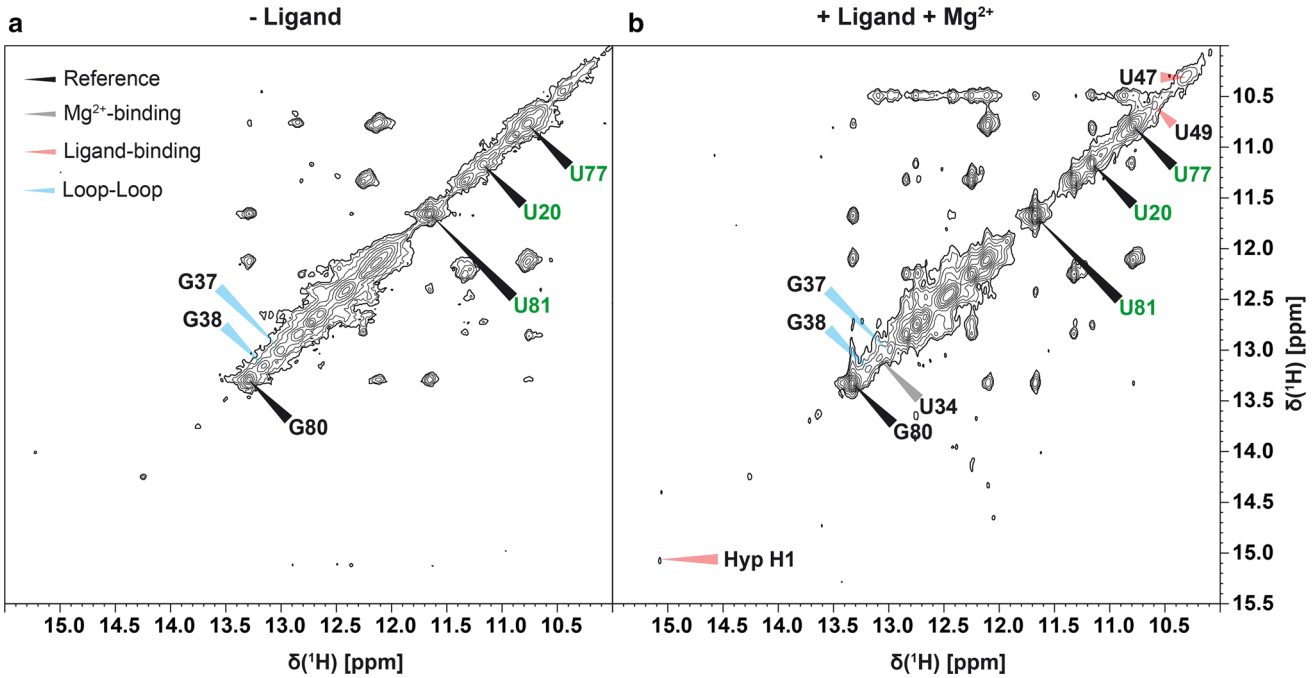

Fig. 6 ^{1}H,^{1}H-NOESY of the ^{19}F-labeled Gsw^{apt} in the absence and presence of ligand at the 600 MHz and 298 K. The ^{1}H pulses were applied on-resonance with the water frequency. For hard ^{1}H pulse, a field strength of 18 kHz was used. For ^{15}N-labeled RNAs, during acquisition, ^{15}N decoupling was achieved by GARP-decoupling. The 2D experiment was recorded, using a frequency jump, with a spectral width of 15 and 25 ppm for the indirect and direct dimension, respectively; 512 and 2048 pts were recorded for t_1 and t_2, respectively. The relaxation delay was set to 1.5 s. The A–U Watson–Crick base paired uridines are labeled in *green*. All other base pairs are indicated in *black*. **a** Spectrum of the G and U imino proton region of the ^{19}F-labeled Gsw^{apt} in the absence of ligand. G80, U81, U20 and U77 are used as reference signals. **b** Spectrum of the G and U imino proton region of the ^{19}F-labeled Gsw^{apt} in the presence of ligand and 2 mM Mg^{2+}. U34 is used as a reference signal for ligand and Mg^{2+}-binding. Ligand binding is monitored by the hypoxanthine H1 signal and two signals from the binding pocket of the RNA (U47 and U49)

spectrum. In comparison to the unlabeled RNA, the imino proton signal of U34 is not shifted in the spectrum of the ^{19}F-labeled Gsw^{apt}. This indicates, that in the ^{19}F-labeled RNA, all uridine imino protons involved in Watson–Crick base pairing to 2F-adenines show an important imino proton shift whereas the imino protons involved in non-canonical base pairings to 2F-adenines do not show an imino proton shift. The ^{19}F-label at the C2 position is therefore Watson–Crick base pair sensitive. The imino proton signals of G37 and G38 are characteristic for the tetrads A33·A66·C60–G38 and U34·A65·C61–G37, which are involved in the "kissing-loop" interaction between the loops L2 and L3. Furthermore, the G37–C61 Watson–Crick base pair and A33 form an adenine specific type II A-minor motif (Appasamy et al. 2013; Batey et al. 2004). The presence of the G37 and G38 imino proton signals in the ^{19}F-labeled RNA suggest that the tetrads and the A-minor motif are unaffected by the ^{19}F-label. We therefore suggest that the 2F-adenine has little to no effect on the stability of this RNA motif within the riboswitch molecule studied here.

Identification of ^{19}F-1D signals

The ^{19}F,^{1}H-HOESYs that were used to correlate the uridine imino protons to the paired adenines are shown in Fig. 7b. As three major uridine signals were observable in the ^{1}H,^{1}H-NOESY, it was expected that the ^{19}F,^{1}H-HOESY showed three major cross signals. In the absence of ligand, U20, U77 and U81 show a clear cross correlation to the pairing A76, A19 and A15, respectively. Upon addition of ligand, a cross signal from U22 to A52 arises. This could be caused by ligand induced stabilization that prevents the imino proton from U22 to be exchanged. The ^{19}F,^{1}H-HOESY also showed cross signals between ^{19}F nuclei and anomeric H1′ protons as was shown before (Scott et al. 2004). Upon ligand binding, the H1′ signals are shifted by $<\Delta\delta^{1}\mathrm{H}> = 0.3$ ppm and the average peak width changes from 0.26 ppm to 0.31 ppm. Also, all signals shift in the same direction, the shift lies within the peak width.

All four cross signals could be assigned to the ^{19}F-1D (Fig. 7c). Upon ligand binding, the signal of A19 is shifted downfield while the signals of A15 and A76 remain

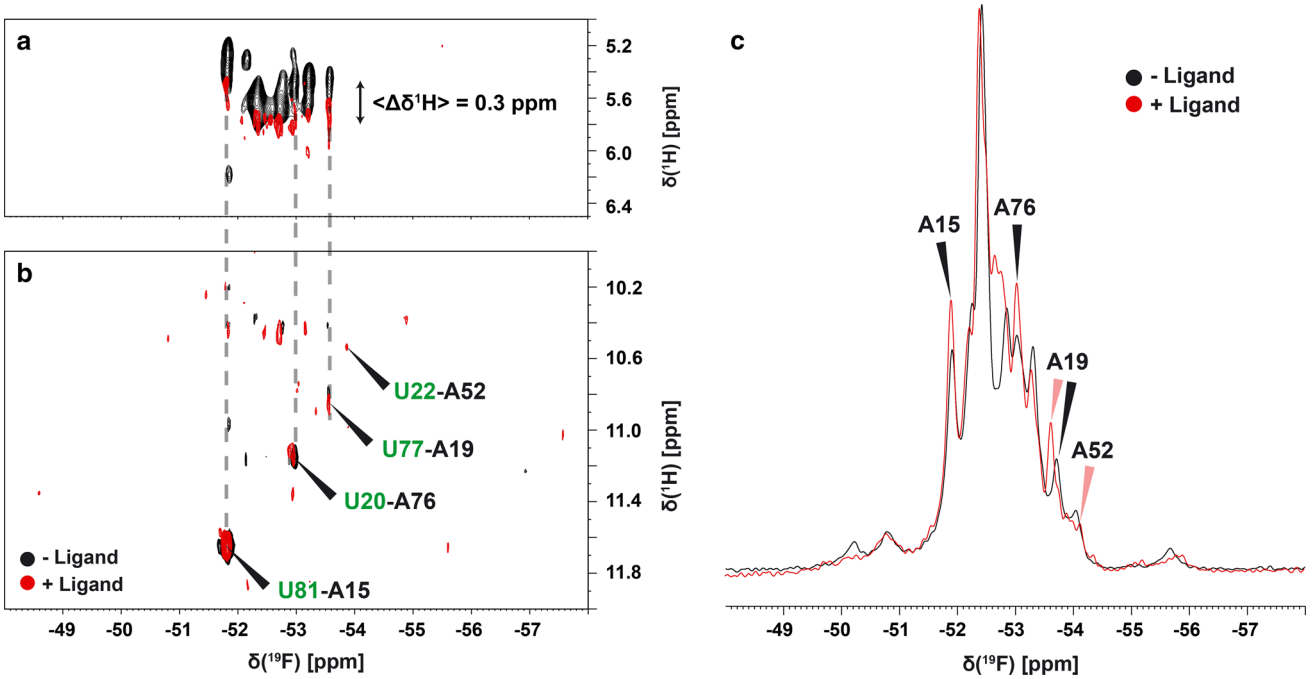

Fig. 7 ^{19}F-correlation spectra of the ^{19}F-labeled Gsw^{apt} in the absence (*black*) and presence (*red*) of ligand. The A-U Watson–Crick base paired uridines are labeled in *green*. The A-U base paired 2F-adenines are labeled in *black*. **a** H1′ signal region of the fluorine detected ^{19}F,^{1}H-HOESY at the 300 MHz at 298 K. The signal shift from ligand unbound to ligand bound is indicated. **b** Imino proton region of the ^{19}F,^{1}H-HOESY in the absence (*black*) and presence (*red*) of the ligand at the 300 MHz at 298 K. The cross signals of the uridine imino protons to the fluorine atom at the 2-position of the canonical paired adenines are indicated (*green*). For the spectra shown in **a** and **b**, the ^{1}H pulses were applied on-resonance with the water frequency. The carrier for ^{19}F was set to −52 ppm. For hard ^{19}F and ^{1}H pulses, field strengths of 23.1 and 22.2 kHz were applied, respectively. The 2D experiment was recorded with a spectral width of 10.5 and 20 ppm for the indirect and direct dimension, respectively; 128 pts and 2048 pts were recorded for t_1 and t_2, respectively. ^{1}H decoupling was achieved using MLEV-sequence. The relaxation delay was set to 2 s. **c** ^{19}F-1D of the ^{19}F-labeled Gsw^{apt} in the absence (*black*) and presence (*red*) of ligand at the 500 MHz at 298 K. The carrier for ^{19}F was set to −52 ppm. For hard ^{19}F pulses, a field strength of 16.7 kHz. The 1D experiment was recorded with a spectral width of 100 ppm with 256 pts. The relaxation delay was set to 1 s. The ^{19}F signals identified using the ^{19}F,^{1}H-HOESY are indicated

unchanged. The signal of A52 is used as a reporter signal for ligand binding to the RNA. The signals rising between −52.5 and −53 ppm at ligand binding could belong to fluorinated adenines situated in and around the binding pocket. The broader minor peaks between −50 and −51.5 ppm signify a conformational diversity which is not detectable in the ^{1}H-spectra. Whether these minor populated conformations are caused by the introduction of the ^{19}F-label or just revealed by the increased chemical shift dispersion remains subject of further investigation.

Conclusion

The use of 2F-ATP for in vitro transcription allows the synthesis of ^{19}F-labeled RNA in high yields, sufficient for NMR samples, and does not change the structural integrity or ligand binding capability of the RNA. By substituting the adenine H1 for a ^{19}F-atom, we were able to show that this non-invasive label selectively shifts the imino proton signals from canonical base pairs. This selective chemical shift change allows the identification of Watson–Crick base paired uridine imino protons making this application ideal for even larger RNAs where the signal overlap in the proton region becomes significant and renders the analysis of the secondary structure difficult. We could furthermore demonstrate that the introduction of 2F-adenine into the RNA does not change the stability of tertiary interactions such as the kissing-loop. However, the here shown tetrad involved a 2F-adenine interacting with a Watson–Crick G–C base pair. In this interaction the ^{19}F-label has the same distance (∼3.2 Å) to the amino group of G37 and the carbonyl group of C61. If the observed effect is different for other base pair compositions needs to be further evaluated. Together with the high incorporation efficiency, the increased resolution within A-form helices makes the 2F-ATP the nucleotide of choice for the uniformly labeling of large RNAs by in vitro transcription.

We further identified ^{19}F-signals situated in the helix P1 stem of the Gsw^{apt} that plays an important role in the fully functional wild type riboswitch where it indicates if the terminator or anti-terminator conformation is adopted. We suggest that the ratio determination of this bistable full length RNA can be done by ^{19}F-NMR using 2F-ATP labels without affecting the ligand binding capability or the conformational equilibrium of the RNA. In the long term, we aim to determine kinetic rates of a bistable RNA systems as was shown in 2014 (Zhao et al. 2014). This could be done with the much larger full length riboswitch utilizing ^{19}F-labeling.

Acknowledgments We thank E. Stirnal for HPLC purification of RNAs. The work was supported within the DFG-funded collaborative research center: SFB902. H.S. is member of the DFG-funded cluster of excellence: macromolecular complexes. BMRZ is supported by the state of Hesse.

References

Alvarado LJ et al (2014) Regio-selective chemical-enzymatic synthesis of pyrimidine nucleotides facilitates RNA structure and dynamics studies. ChemBioChem 15:1573–1577. doi:10.1002/cbic.201402130

Appasamy D, Ramlan EI, Firdaus-Raih M (2013) Comparative sequence and structure analysis reveals the conservation and diversity of nucleotide positions and their associated tertiary interactions in the riboswitches. PLoS One. doi:10.1371/journal.pone.0073984

Baldo JH, Hansen PE, Shriver JW, Sykes BD (1983) 2-Fluoro-Atp, a fluorinated Atp Analog: F-19 nuclear magnetic-resonance studies of the 2-fluoro-Adp. Myosin subfragment-1 complex. Can J Biochem Cell B 61:115–119

Batey RT, Inada M, Kujawinski E, Puglisi JD, Williamson JR (1992) Preparation of isotopically labeled ribonucleotides for multidimensional NMR-spectroscopy of RNA. Nucleic Acids Res 20:4515–4523. doi:10.1093/nar/20.17.4515

Batey RT, Gilbert SD, Montange RK (2004) Structure of a natural guanine-responsive riboswitch complexed with the metabolite hypoxanthine. Nature 432:411–415. doi:10.1038/nature03037

Battaglia MR, Buckingham AD, Williams JH (1981) The electric quadrupole-moments of benzene and hexafluorobenzene. Chem Phys Lett 78:420–423

Broom AD, Amarnath V, Vince R, Brownell J (1979) Poly(2-fluoroadenylic acid). The role of basicity in the stabilization of complementary helices. Biochim Biophys Acta 563:508–517

Buck J, Furtig B, Noeske J, Wohnert J, Schwalbe H (2007) Time-resolved NMR methods resolving ligand-induced RNA folding at atomic resolution. Proc Natl Acad Sci USA 104:15699–15704. doi:10.1073/pnas.0703182104

Buck J, Noeske J, Wohnert J, Schwalbe H (2010) Dissecting the influence of Mg2+ on 3D architecture and ligand-binding of the guanine-sensing riboswitch aptamer domain. Nucleic Acids Res 38:4143–4153. doi:10.1093/nar/gkq138

Butcher SE, Allain FHT, Feigon J (2000) Determination of metal ion binding sites within the hairpin ribozyme domains by NMR. Biochemistry 39:2174–2182. doi:10.1021/Bi9923454

Carlomagno T, Amata I, Codutti L, Falb M, Fohrer J, Masiewicz P, Simon B (2013) Structural principles of RNA catalysis in a 2′–5′ lariat-forming ribozyme. J Am Chem Soc 135:4403–4411. doi:10.1021/Ja311868t

Cavaluzzi MJ, Borer PN (2004) Revised UV extinction coefficients for nucleoside-5′-monophosphates and unpaired DNA and RNA. Nucleic Acids Res. doi:10.1093/nar/gnh015

Chowdhury S, Maris C, Allain FHT, Narberhaus F (2006) Molecular basis for temperature sensing by an RNA thermometer. EMBO J 25:2487–2497. doi:10.1038/sj.emboj.7601128

Christiansen LC, Schou S, Nygaard P, Saxild HH (1997) Xanthine metabolism in *Bacillus subtilis*: characterization of the xpt–pbuX operon and evidence for purine- and nitrogen-controlled expression of genes involved in xanthine salvage and catabolism. J Bacteriol 179:2540–2550

Codington JF, Fox JJ, Doerr IL (1964) Nucleosides. 18. Synthesis of 2]-fluorothymidine 2]-fluorodeoxyuridine + other 2]-halogeno-2]-deoxy nucleosides. J Org Chem 29:558–564. doi:10.1021/Jo01026a009

Davis JH, Tonelli M, Scott LG, Jaeger L, Williamson JR, Butcher SE (2005) RNA helical packing in solution: NMR structure of a 30 kDa GAAA tetraloop-receptor complex. J Mol Biol 351:371–382. doi:10.1016/j.jmb.2005.05.069

Dayie KT, Tolbert TJ, Williamson JR (1998) 3D C(CC)H TOCSY experiment for assigning protons and carbons in uniformly C-13- and selectively H-2-labeled RNA. J Magn Reson 130:97–101. doi:10.1006/jmre.1997.1286

D'Souza V, Dey A, Habib D, Summers MF (2004) NMR structure of the 101-nucleotide core encapsidation signal of the Moloney murine leukemia virus. J Mol Biol 337:427–442. doi:10.1015/j.jmb.2004.01.037

Duszczyk MM, Wutz A, Rybin V, Sattler M (2011) The Xist RNA A-repeat comprises a novel AUCG tetraloop fold and a platform for multimerization. RNA 17:1973–1982. doi:10.1261/Rna.2747411

Fauster K, Kreutz C, Micura R (2012) 2′-SCF3 uridine-a powerful label for probing structure and function of RNA by 19F NMR spectroscopy. Angew Chem Int Ed Engl 51:13080–13084. doi:10.1002/anie.201207128

Ferner J et al (2009) Structures of HIV TAR RNA-ligand complexes reveal higher binding stoichiometries. ChemBioChem 10:1490–1494. doi:10.1002/cbic.200900220

Furtig B, Richter C, Wohnert J, Schwalbe H (2003) NMR spectroscopy of RNA. Chembiochem 4:936–962. doi:10.1002/cbic.200300700

Furtig B, Richter C, Schell P, Wenter P, Pitsch S, Schwalbe H (2008) NMR-spectroscopic characterization of phosphodiester bond cleavage catalyzed by the minimal hammerhead ribozyme. RNA Biol 5:41–48

Garavis M et al (2014) Discovery of selective ligands for telomeric RNA G-quadruplexes (TERRA) through 19F-NMR based fragment screening. ACS Chem Biol 9:1559–1566. doi:10.1021/cb500100z

Geen H, Freeman R (1991) Band-selective radiofrequency pulses. J Magn Reson 93:93–141. doi:10.1016/0022-2364(91)90034-Q

Graber D, Moroder H, Micura R (2008) 19F NMR spectroscopy for the analysis of RNA secondary structure populations. J Am Chem Soc 130:17230–17231. doi:10.1021/ja806716s

Granqvist L, Virta P (2014) 4′-C-[(4-trifluoromethyl-1H-1,2,3-triazol-1-yl)methyl]thymidine as a sensitive (19)F NMR sensor for the detection of oligonucleotide secondary structures. J Org Chem 79:3529–3536. doi:10.1021/jo500326j

Guillerez J, Lopez PJ, Proux F, Launay H, Dreyfus M (2005) A mutation in T7 RNA polymerase that facilitates promoter clearance. Proc Natl Acad Sci USA 102:5958–5963. doi:10.1073/pnas.0407141102

Horowitz J, Ou CN, Ishaq M (1974) Isolation and partial characterization of *Escherichia coli* valine transfer RNA with uridine-derived residues replaced by 5-fluorouridine. J Mol Biol 88:301–312

Houck-Loomis B, Durney MA, Salguero C, Shankar N, Nagle JM, Goff SP, D'Souza VM (2011) An equilibrium-dependent retroviral mRNA switch regulates translational recoding. Nature 480:561–564. doi:10.1038/Nature10657

Huang P, Plunkett W (1987) Phosphorolytic cleavage of 2-fluoroadenine from 9-beta-D-arabinofuranosyl-2-fluoroadenine by *Escherichia-Coli:* a pathway for 2-fluoro-Atp production. Biochem Pharmacol 36:2945–2950. doi:10.1016/0006-2952(87)90207-3

Keane SC et al (2015) Structure of the HIV-1 RNA packaging signal. Science 348:917–921. doi:10.1126/science.aaa9266

Kiviniemi A, Virta P (2010) Characterization of RNA invasion by (19)F NMR spectroscopy. J Am Chem Soc 132:8560–8562. doi:10.1021/ja1014629

Kiviniemi A, Virta P (2011) Synthesis of aminoglycoside-3′-conjugates of 2′-O-methyl oligoribonucleotides and their invasion to a 19F labeled HIV-1 TAR model. Bioconjug Chem 22:1559–1566. doi:10.1021/bc200101r

Kiviniemi A, Murtola M, Ingman P, Virta P (2013) Synthesis of fluorine-labeled peptide nucleic acid building blocks as sensors for the 19F NMR spectroscopic detection of different hybridization modes. J Org Chem 78:5153–5159. doi:10.1021/jo400014y

Kline PC, Serianni AS (1990) C-13-Enriched ribonucleosides: synthesis and application of C-13-H-1 and C-13-C-13 spin-coupling constants to assess furanose and N-glycoside bond conformations. J Am Chem Soc 112:7373–7381. doi:10.1021/Ja00176a043

Kosutic M et al (2014) Surprising base pairing and structural properties of 2′-trifluoromethylthio-modified ribonucleic acids. J Am Chem Soc 136:6656–6663. doi:10.1021/ja5005637

Kreutz C, Kahlig H, Konrat R, Micura R (2005) Ribose 2′-F labeling: a simple tool for the characterization of RNA secondary structure equilibria by 19F NMR spectroscopy. J Am Chem Soc 127:11558–11559. doi:10.1021/ja052844u

Kreutz C, Kahlig H, Konrat R, Micura R (2006) A general approach for the identification of site-specific RNA binders by 19F NMR spectroscopy: proof of concept. Angew Chem Int Ed Engl 45:3450–3453. doi:10.1002/anie.200504174

Lescoute A, Westhof E (2006) The A-minor motifs in the decoding recognition process. Biochimie 88:993–999. doi:10.1016/j.biochi.2006.05.018

Levitt MH, Freeman R (1981) Composite pulse decoupling. J Magn Reson 43:502–507. doi:10.1016/0022-2364(81)90066-4

Lombes T et al (2012) Investigation of RNA-ligand interactions by 19F NMR spectroscopy using fluorinated probes. Angew Chem Int Ed Engl 51:9530–9534. doi:10.1002/anie.201204083

Mandal M, Boese B, Barrick JE, Winkler WC, Breaker RR (2003) Riboswitches control fundamental biochemical pathways in *Bacillus subtilis* and other bacteria. Cell 113:577–586

Marchanka A, Simon B, Althoff-Ospelt G, Carlomagno T (2015) RNA structure determination by solid-state NMR spectroscopy. Nat Commun. doi:10.1038/Ncomms8024

Milligan JF, Groebe DR, Witherell GW, Uhlenbeck OC (1987) Oligoribonucleotide synthesis using T7 RNA polymerase and synthetic DNA templates. Nucleic Acids Res 15:8783–8798

Mori S, Abeygunawardana C, Johnson MO, van Zijl PC (1995) Improved sensitivity of HSQC spectra of exchanging protons at short interscan delays using a new fast HSQC (FHSQC) detection scheme that avoids water saturation. J Magn Reson B 108:94–98

Nahvi A, Sudarsan N, Ebert MS, Zou X, Brown KL, Breaker RR (2002) Genetic control by a metabolite binding mRNA. Chem Biol 9:1043

Neuner S, Santner T, Kreutz C, Micura R (2015) The "speedy" synthesis of atom-specific N-15 imino/amido-labeled RNA. Chem-Eur J 21:11634–11643. doi:10.1002/chem.201501275

Nikonowicz EP, Sirr A, Legault P, Jucker FM, Baer LM, Pardi A (1992) Preparation of C-13 and N-15 Labeled Rnas for Heteronuclear Multidimensional Nmr-Studies. Nucleic Acids Res 20:4507–4513. doi:10.1093/nar/20.17.4507

Nissen P, Ippolito JA, Ban N, Moore PB, Steitz TA (2001) RNA tertiary interactions in the large ribosomal subunit: the A-minor motif. Proc Natl Acad Sci USA 98:4899–4903. doi:10.1073/pnas.081082398

Noeske J, Richter C, Grundl MA, Nasiri HR, Schwalbe H, Wohnert J (2005) An intermolecular base triple as the basis of ligand specificity and affinity in the guanine- and adenine-sensing riboswitch RNAs. Proc Natl Acad Sci USA 102:1372–1377. doi:10.1073/pnas.0406347102

Olsen GL, Edwards TE, Deka P, Varani G, Sigurdsson ST, Drobny GP (2005) Monitoring tat peptide binding to TAR RNA by solid-state 31P-19F REDOR NMR. Nucleic Acids Res 33:3447–3454. doi:10.1093/nar/gki626

Piotto M, Saudek V, Sklenar V (1992) Gradient-tailored excitation for single-quantum NMR spectroscopy of aqueous solutions. J Biomol NMR 2:661–665

Puffer B, Kreutz C, Rieder U, Ebert MO, Konrat R, Micura R (2009) 5-Fluoro pyrimidines: labels to probe DNA and RNA secondary structures by 1D 19F NMR spectroscopy. Nucleic Acids Res 37:7728–7740. doi:10.1093/nar/gkp862

Quant S et al (1994) Chemical synthesis of C-13-labeled monomers for the solid-phase and template controlled enzymatic-synthesis of DNA and RNA oligomers. Tetrahedron Lett 35:6649–6652. doi:10.1016/S0040-4039(00)73458-7

Reif B et al (1997) Structural comparison of oligoribonucleotides and their 2′-deoxy-2′-fluoro analogs by heteronuclear NMR spectroscopy. Helv Chim Acta 80:1952–1971. doi:10.1002/hlca.19970800614

Rinnenthal J, Klinkert B, Narberhaus F, Schwalbe H (2010) Direct observation of the temperature-induced melting process of the Salmonella fourU RNA thermometer at base-pair resolution. Nucleic Acids Res 38:3834–3847. doi:10.1093/nar/gkq124

Rinnenthal J, Buck J, Ferner J, Wacker A, Furtig B, Schwalbe H (2011) Mapping the landscape of RNA dynamics with NMR spectroscopy. Acc Chem Res 44:1292–1301. doi:10.1021/ar200137d

Sashital DG, Cornilescu G, Butcher SE (2004) U2-U6 RNA folding reveals a group II intron-like domain and a four-helix junction. Nat Struct Mol Biol 11:1237–1242. doi:10.1038/Nsmb863

Schwalbe H, Buck J, Furtig B, Noeske J, Wohnert J (2007) Structures of RNA switches: insight into molecular recognition and tertiary structure. Angew Chem Int Ed Engl 46:1212–1219. doi:10.1002/anie.200604163

Scott LG, Geierstanger BH, Williamson JR, Hennig M (2004) Enzymatic synthesis and F-19 NMR studies of 2-fluoroadenine-substituted RNA. J Am Chem Soc 126:11776–11777. doi:10.1021/Ja047556x

Serganov A et al (2004) Structural basis for discriminative regulation of gene expression by adenine- and guanine-sensing mRNAs. Chem Biol 11:1729–1741. doi:10.1016/j.chembiol.2004.11.018

Shaka AJ, Barker PB, Freeman R (1985) Computer-optimized decoupling scheme for wideband applications and low-level operation. J Magn Reson 64:547–552. doi:10.1016/0022-2364(85)90122-2

Sklenar V, Bax A (1987) Spin-echo water suppression for the generation of pure-phase two-dimensional NMR-spectra. J Magn Reson 74:469–479. doi:10.1016/0022-2364(87)90269-1

Sklenar V, Piotto M, Leppik R, Saudek V (1993) Gradient-tailored water suppression for H-1-N-15 Hsqc experiments optimized to retain full sensitivity. J Magn Reson Ser A 102:241–245. doi:10.1006/jmra.1993.1098

Staple DW, Butcher SE (2003) Solution structure of the HIV-1 frameshift inducing stem-loop RNA. Nucleic Acids Res 31:4326–4331. doi:10.1093/Nar/Gkg654

Suck D, Saenger W, Main P, Germain G, Declercq JP (1974) X-ray structure of 3′,5′-diacetyl-2′-deoxy-2′-fluorouridine: a pyrimidine nucleoside in the syn conformation. Biochim Biophys Acta 361:257–265

Thakur CS, Dayie TK (2012) Asymmetry of C-13 labeled 3-pyruvate affords improved site specific labeling of RNA for NMR spectroscopy. J Biomol NMR 52:65–77. doi:10.1007/s10858-011-9582-5

Wacker A, Buck J, Mathieu D, Richter C, Wohnert J, Schwalbe H (2011) Structure and dynamics of the deoxyguanosine-sensing riboswitch studied by NMR-spectroscopy. Nucleic Acids Res 39:6802–6812. doi:10.1093/nar/gkr238

Wacker A, Buck J, Richter C, Schwalbe H, Wohnert J (2012) Mechanisms for differentiation between cognate and near-cognate ligands by purine riboswitches. RNA Biol 9:672–680. doi:10.4161/rna.20106

Wenter P, Reymond L, Auweter SD, Allain FHT, Pitsch S (2006) Short, synthetic and selectively C-13-labeled RNA sequences for the NMR structure determination of protein-RNA complexes. Nucleic Acids Res. doi:10.1093/nar/gkl427

Yu C, Levy GC (1984) Two-dimensional heteronuclear NOE (HOESY) experiments: investigation of dipolar interactions between heteronuclei and nearby protons. J Am Chem Soc 106:6533–6537. doi:10.1021/Ja00334a013

Zhao C, Devany M, Greenbaum NL (2014) Measurement of chemical exchange between RNA conformers by (19)F NMR. Biochem Biophys Res Commun 453:692–695. doi:10.1016/j.bbrc.2014.09.075